Sensorless Induction Motor Drives Using Adaptive Flux Observer at Low Frequencies

Mohamed S. Zaky

Department of Electrical
Engineering
Northern Border University
Arar, Saudi Arabia
mszaky78@yahoo.com

Hady Abdel Maksoud

Department of Electrical
Engineering
Minoufiya University
Shebin El-Kom, Egypt
hady_elgendy@yahoo.com

Haitham Z. Azazi

Department of Electrical
Engineering
Minoufiya University
Shebin El-Kom, Egypt
haitham_azazi@yahoo.com

Abstract—**Operation at low frequencies of sensorless drives using machine model-based estimation methods is a challenging issue. This paper proposes an adaptive flux observer (AFO) method of speed estimation for sensorless Induction Motor (IM) drives. The observer feedback gains are designed to guarantee accurate speed estimation, especially at low frequencies in the regenerating mode operation. A complete sensorless IM drive with the proposed AFO is executed in the laboratory. Extensive experimental results under different operating conditions are provided to prove the effectiveness of the proposed AFO, particularly under low stator frequencies in both motoring and regenerating modes of operation.**

Keywords-sensorless control; induction motors; adaptive flux observer; low frequencies; observer feedback gain

I.   INTRODUCTION

Precise speed information is very important for speed control of Induction Motor (IM) drives. Direct speed sensors or encoders are used for speed measurements. However, they have several disadvantages such as extra cost, extra space, extra wiring, careful mounting, and additional electronics. Therefore, speed estimation methods of sensorless IM drives were developed to replace the direct speed sensors. The sensorless drives are characterized by low cost, high reliability, decreased size, less maintenance, less wiring, and decreased complexity [1]. Many speed estimation methods have been presented in the literature. They can be classified into two categories. The non-fundamental wave speed estimation methods are a good choice at zero and very low stator frequencies. They are independent of parameters variation. However, they increase the ripples and need special machine design. Fundamental-wave-model-based approaches of speed estimation give good behavior during medium and high frequencies. However, they fail to guarantee the desired performance under very low and zero speeds [2]. They are highly dependent on the machine parameters, the back emf, inverter nonlinearity, and errors of the data acquisition converters. Different speed estimation methods with and without parameters estimations were presented [3-8]. These methods can be classified as different estimation methods such as direct speed calculation method, model reference adaptive

system method (MRAS) [1], Kalman filter [2], adaptive flux observers (AFO) [3, 6, 7], intelligent control based methods (AI) [5], and sliding mode observer (SMO) [8]. Non-fundamental wave speed estimation methods are a good choice at zero and very low stator frequencies [9]. They are independent of parameter variations. High frequency voltage injections are one class of these methods. Numerous attempts and efforts were extensively proposed in [9-20]. In [9], a multiphase induction machine was utilized to obtain larger slotting harmonic magnitude compared to normal three phase induction machines. The machine slotting signal depends on the rotor slot type and bars. However, this method suffers from increasing the stator copper losses due to increasing the principle rotor slot losses. The transient voltage excitation using INFORM technique for sensorless speed estimation under very low and zero speed operation was addressed in [10]. High frequency injection (HFI) methods were used to energize the stator voltage with high frequency signal. The machine current components were utilized to estimate the rotor speed and angles using different separation algorithms as in [11-16]. To improve the performance of sensorless drive method based high sinusoidal voltage injection with high frequency, the square wave voltage injection schemes were utilized [17-19]. In [17-18], the conventional square voltage injection scheme needs high carrier signals with high frequency. A novel square wave carrier signal injection to overcome the disadvantages of the conventional ones was addressed in [19]. Also, zero voltage vector injection scheme for online flux estimation was presented in [20]. However, these methods have torque ripples and need a special design of the machine.

AFO needs estimation of the machine parameters, especially at very low frequencies because the back emf is very low and the voltage drop on the stator resistance has a major effect. Therefore, the sensorless control system with parameter estimation was designed as multiple-input-multiple output [3, 5, 6], or needs the designing of three estimators as independent single-input-single output systems as in [7]. Therefore, this estimation complicated the sensorless drive systems. Another problem is that the machine model-based methods of sensorless drives are incapable of operating stably during a long time under rated load at zero stator frequency. This instability is

maximized at regenerative mode of operation in the very low speed region [21-23].

This study's key goals can be summarized as follow:

1) Proposing AFO for sensorless IM drives.
2) Designing of observer feedback gains for stable operation of AFO at low frequencies based on Lyapunov Theory.
3) Execution of the complete sensorless IM using AFO algorithm in the laboratory using DSP-DS1104 control board.
4) Experimental results at low frequencies should verify the applicability of the proposed method.

II.   IM AND OBSERVER MODELS

The dynamic d-q model of the IM is described by stationary reference frame using (1).

$$
\left.
\begin{aligned}
p i_{ds}^s &= b v_{ds}^s + a i_{ds}^s + c \lambda_{dr}^s + d \omega_r \lambda_{qr}^s \\
p i_{qs}^s &= b v_{qs}^s + a i_{qs}^s + c \lambda_{qr}^s - d \omega_r \lambda_{dr}^s \\
p \lambda_{dr}^s &= g i_{ds}^s - \omega_r \lambda_{qr}^s - f \lambda_{dr}^s \\
p \lambda_{qr}^s &= g i_{qs}^s + \omega_r \lambda_{dr}^s - f \lambda_{qr}^s
\end{aligned}
\right\} \tag{1}
$$

where,

$$
a = -\left(\frac{R_s}{\sigma L_s} + \frac{L_m^2}{\sigma L_s T_r L_r} \right), \quad c = \frac{1}{\varepsilon T_r}, \quad d = \frac{1}{\varepsilon}, \quad g = \frac{L_m}{T_r}
$$

$$
\varepsilon = \frac{\sigma L_s L_r}{L_m}, \quad b = \frac{1}{\sigma L_s}, \quad \sigma = 1 - \frac{L_m^2}{L_s L_r}, \quad T_r = \frac{L_r}{R_r}, \quad f = \frac{1}{T_r}
$$

and,

$$\vec{v}_s^s = \begin{bmatrix} v_{ds}^s & v_{qs}^s \end{bmatrix}^T \qquad \text{is dq stator voltage,}$$

$$\vec{i}_s^s = \begin{bmatrix} i_{ds}^s & i_{qs}^s \end{bmatrix}^T \qquad \text{is dq stator current,}$$

$$\vec{i}_r^s = \begin{bmatrix} i_{dr}^s & i_{qr}^s \end{bmatrix}^T \qquad \text{is dq rotor current,}$$

$$\vec{\lambda}_s^s = \begin{bmatrix} \lambda_{ds}^s & \lambda_{qs}^s \end{bmatrix}^T \qquad \text{is dq stator flux,}$$

$$\vec{\lambda}_r^s = \begin{bmatrix} \lambda_{dr}^s & \lambda_{qr}^s \end{bmatrix}^T \qquad \text{is dq rotor flux,}$$

R_s, R_r are the stator and rotor resistances, L_m, L_s, L_r are magnetizing inductance, stator inductance, and the rotor inductance, respectively, ω_r is the rotor speed, J is the moment of inertia, and B is the viscous friction. The schematic diagram of IFOC for IM with the AFO is clarified in Figure 1.

Fig. 1.   The schematic diagram of IFOC for an IM with the AFO.

III.   DESIGN OF AN ADAPTIVE FLUX OBSERVER

A. Structure of an Adaptive Flux Observer

An AFO is described by a stationary reference frame based on (1) using (2):

$$
\left.
\begin{aligned}
p \hat{i}_{ds}^s &= b v_{ds}^s + a \hat{i}_{ds}^s + c \hat{\lambda}_{dr}^s + d \hat{\omega}_r \hat{\lambda}_{qr}^s + K_1 e_{id} \\
p \hat{i}_{qs}^s &= b v_{qs}^s + a \hat{i}_{qs}^s + c \hat{\lambda}_{qr}^s - d \hat{\omega}_r \hat{\lambda}_{dr}^s + K_2 e_{iq} \\
p \hat{\lambda}_{dr}^s &= g \hat{i}_{ds}^s - \hat{\omega}_r \hat{\lambda}_{qr}^s - f \hat{\lambda}_{dr}^s \\
p \hat{\lambda}_{qr}^s &= g \hat{i}_{qs}^s + \hat{\omega}_r \hat{\lambda}_{dr}^s - f \hat{\lambda}_{qr}^s
\end{aligned}
\right\} \tag{2}
$$

where, K_1 and K_2 are the current and flux observer gains,

$e_{id} = \hat{i}_{ds}^s - i_{ds}^s$ and $e_{iq} = \hat{i}_{qs}^s - i_{qs}^s$.

Using (1) and (2), the current and flux errors are derived as follows.

$$
\left.
\begin{aligned}
p e_{id} &= a e_{id} + c e_{\lambda d} + d \omega_r e_{\lambda q} + d \hat{\lambda}_{qr}^s \Delta \omega_r + K_1 e_{id} \\
p e_{iq} &= a e_{iq} + c e_{\lambda q} - d \omega_r e_{\lambda d} - d \hat{\lambda}_{dr}^s \Delta \omega_r + K_2 e_{iq} \\
p e_{\lambda d} &= e e_{id} - \omega_r e_{\lambda q} - \hat{\lambda}_{qr}^s \Delta \omega_r - f e_{\lambda d} \\
p e_{\lambda q} &= e e_{iq} + \omega_r e_{\lambda d} + \hat{\lambda}_{dr}^s \Delta \omega_r - f e_{\lambda q}
\end{aligned}
\right\} \tag{3}
$$

where,

$\Delta \omega_r = \omega_r - \hat{\omega}_r$,

$e_{\lambda d} = \hat{\lambda}_{dr}^s - \lambda_{dr}^s$,

$e_{\lambda q} = \hat{\lambda}_{qr}^s - \lambda_{qr}^s$.

It is important to design the observer gains K_1 and K_2 of the current observer to ensure the system stability.

Proof 1: The Lyapunov function can be selected as (4):

$$V = \frac{1}{2}e_{id}^{\;2} + \frac{1}{2}e_{iq}^{\;2} \qquad (4)$$

The first derivative is expressed as (5).

$$\dot{V} = e_{id}\dot{e}_{id} + e_{iq}\dot{e}_{iq}$$

$$= \begin{cases} e_{id}\left(ae_{id} + ce_{\lambda d} + d\omega_r e_{\lambda q} + d\hat{\lambda}_{qr}^s \Delta\omega_r + K_1 e_{id}\right) \\ e_{iq}\left(ae_{iq} + ce_{\lambda q} - d\omega_r e_{\lambda d} - d\hat{\lambda}_{dr}^s \Delta\omega_r + K_2 e_{iq}\right) \end{cases} \qquad (5)$$

The sufficient conditions, to guarantee the stability of the current observer using Lyapunov theory, are that a negative definite $\dot{V}$ is obtained. It is found that $e_{id}ae_{id}$ and $e_{iq}ae_{iq}$ are negative. Consequently, the remaining terms of (5) should be negative to ensure the stability.

$$\begin{cases} e_{id}\left(ce_{\lambda d} + d\omega_r e_{\lambda q} + d\hat{\lambda}_{qr}^s \Delta\omega_r + K_1 e_{id}\right) < 0 \\ e_{iq}\left(ce_{\lambda q} - d\omega_r e_{\lambda d} - d\hat{\lambda}_{dr}^s \Delta\omega_r + K_2 e_{iq}\right) < 0 \end{cases} \qquad (6)$$

Then, one can obtain,

$$\begin{cases} \left(\left|ce_{\lambda d} + d\omega_r e_{\lambda q} + d\hat{\lambda}_{qr}^s \Delta\omega_r\right| + \left|K_1 e_{id}\right|\right) < 0 \\ \left(\left|ce_{\lambda q} - d\omega_r e_{\lambda d} - d\hat{\lambda}_{dr}^s \Delta\omega_r\right| + \left|K_2 e_{iq}\right|\right) < 0 \end{cases} \qquad (7)$$

To satisfy the inequality of (7), K_1 and K_2 are designed as (8).

$$\begin{cases} K_1 < -\dfrac{\left|ce_{\lambda d} + d\omega_r e_{\lambda q} + d\hat{\lambda}_{qr}^s \Delta\omega_r\right|}{\left|e_{id}\right|} \\[2mm] K_2 < -\dfrac{\left|ce_{\lambda q} - d\omega_r e_{\lambda d} - d\hat{\lambda}_{dr}^s \Delta\omega_r\right|}{\left|e_{iq}\right|} \end{cases} \qquad (8)$$

The inequalities of (8) can be realized by selecting the values of K_1 and K_2 by (9).

$$\begin{cases} K_1 = k_1 - \dfrac{\left|ce_{\lambda d} + d\omega_r e_{\lambda q} + d\hat{\lambda}_{qr}^s \Delta\omega_r\right|}{\left|e_{id}\right|} \\[2mm] K_2 = k_2 - \dfrac{\left|ce_{\lambda q} - d\omega_r e_{\lambda d} - d\hat{\lambda}_{dr}^s \Delta\omega_r\right|}{\left|e_{iq}\right|} \end{cases} \qquad (9)$$

where, k_1 and k_2 are negative numbers.

IV. EXPERIMENTAL RESULTS

The layout of the experimental system based on a DSP-DS1104 is demonstrated in Figure 2. It assembles from hardware and software components. The hardware components include a 1.1 kW IM interfaced with DC generator for load torque applications, PWM inverter with six IGBT's, gate drive and interface circuits, 3-phase full wave rectifier circuit, DSP-DS1104 control board, incremental encoder, voltage and

current sensors, and personal computer. An encoder to measure the speed is utilized for comparison purpose with estimated speed. The parameters of the IM are shown in Table I. The software components incorporate the Matlab/Simulink for model implementation and the dSPACE software. The effectiveness of the AFO for speed estimation is proved and tested. The practical tests are demonstrated under different operating conditions to certify the sensorless IM drive using the AFO.
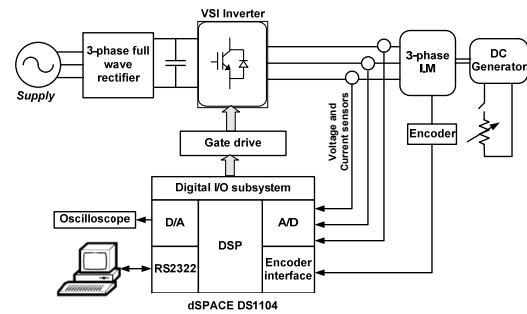
Fig. 2.   The layout of the experimental system based on a DSP-DS1104.

TABLE I.   PARAMETERS OF IM

Rated power	1.1 kW	Stator resistance	7.4826 ohm
Supply voltage	380 volts	Rotor resistance	3.6840 ohm
Rated current	2.545 Amp	Rotor leakage inductance	0.0221 H
No. of poles	4	Stator leakage inductance	0.0221 H
Supply frequency	50 Hz	Mutual inductance	0.4114 H
		Inertia	0.02 kg.m^2

A. Fast Speed Reversal

Figure 3 displays the practical tests of the reference and measured speeds. The figure shows the reference and measured speeds, the quadrature current, i_{qs}, and the dq rotor fluxes. The sensorless IM drive operates at reference speed of 6.28 rad/sec. The step torque of +7N.m is varied at t=1.5sec. Then, the reference speed is changed to −6.28rad/sec at t=3.75sec. The torque is removed at t=7.5 sec. The IM operates in the motoring mode (forward) during t=0 to 1.5sec at no-load and with loading of +7N.m at t=1.5sec to t=3.75sec. The IM operates in the regenerating mode during t=3.75 to 7.5sec with negative speed and positive load. The IM operates in the motoring mode (reverse) during t=7.5 to 12sec with no-load. It is seen that the measured speed and the estimated one are in a good convergence.

B. Slow Speed Reversal

Figure 4 displays the practical tests of the reference and measured speeds, the quadrature current, i_{qs}, and the dq rotor fluxes under slow speed reversal. The speed reference of 10rad/sec is changed slowly to −10rad/sec with load torque change of +7N.m applied at t=1sec. As noted, the estimated speed is stable during the slow speed reversal, especially during the zero crossing point.
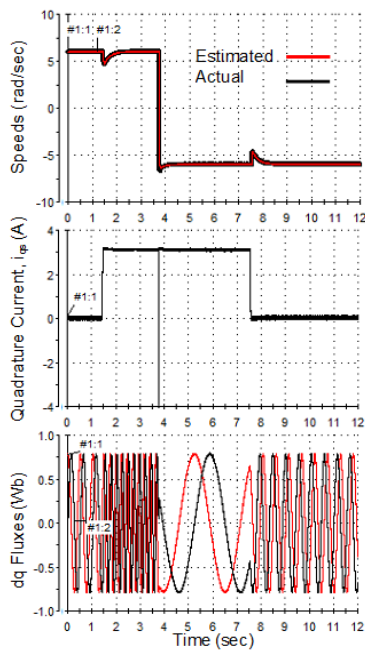
Fig. 3.   The practical tests of the reference and measured speeds, the quadrature current, i_{qs}, and the dq rotor fluxes under fast speed reversal from 6.28rad/sec to −6.28rad/sec. Positive torque of +7N.m applied at t=1.5sec and removed at 7.5sec.
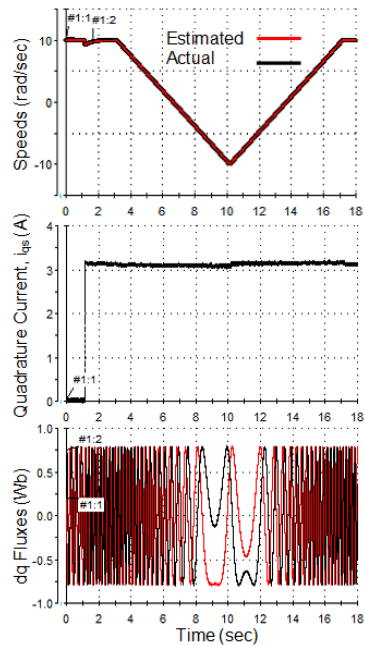
Fig. 4.   The practical tests of the reference and measured speeds, the quadrature current, iqs, and the dq rotor fluxes under slow speed reversal from 10rad/sec to −10rad/sec. Positive torque of +7N.m applied at t=1sec.

C. Low Speed During Regenerating Mode

The practical tests of reference and measured speeds, quadrature current, i_{qs}, and dq rotor fluxes in regenerating mode at low speed with the proposed gains are illustrated in Figure 5.

The speed reference is adjusted at 14rad/sec, then, a torque of −7N.m is applied at t=3.9sec. As noted, a stable sensorless drive is maintained.

D. Low Speed During Motoring Mode

The practical tests of the reference and measured speeds, the quadrature current, i_{qs}, and the dq rotor fluxes during low speed in the motoring mode are presented with the proposed gains. Figure 6 shows the speed reference of 14rad/sec with torque change of +7N.m applied at t=2.4 sec. Practical tests reveal that the designed AFO with the proposed feedback gains guarantees a stable operation in the low speed in both motoring and regenerating modes of operation. Also, the estimated speed has a significant convergence with the measured speed during fast and slow speed reversal.
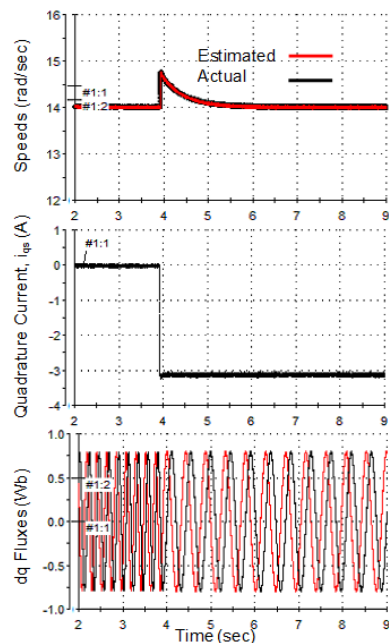
Fig. 5.   The practical tests of the reference and measured speeds, the quadrature current, iqs, and the dq rotor fluxes under low speed regenerating mode of operation at 14 rad/sec. Negative torque of −7 N.m applied at t=3.9 sec.

V. CONCLUSION

The sensorless IM drives using AFO-based speed estimation method was successfully implemented in real-time for low frequency operation. The observer gains were calculated using Lyapunov stability theory. The sensorless IM drive were carried out using DSP-DS1104 platform, and it was examined under different operating conditions, especially at low frequencies in the motoring and regenerating modes of operation. It has been found that the estimated speed has a good convergence with the measured speed. Moreover, the estimated speed tracks smoothly the measured speed during fast and slow speed change. This confirms that the designed feedback gains guarantees the efficacy of the designed AFO, particularly at low frequencies.
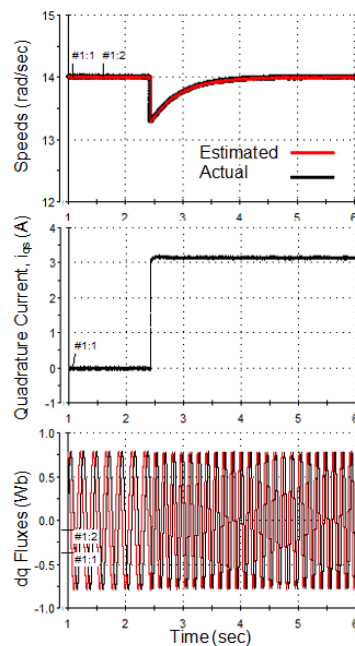
Fig. 6.   The practical tests of the reference and measured speeds, the quadrature current, i_{qs}, and the dq rotor fluxes under low speed motoring mode of operation at 14rad/sec. Positive rated load torque of +7N.m applied at t=2.4sec.

REFERENCES

[1] R. Kumar, S. Das, A. Chattopadhyay, "Comparative assessment of two different model reference adaptive system schemes for speed-sensorless control of induction motor drives", IET Electric Power Applications, Vol. 10, No. 2, pp. 141-154, 2016

[2] Z. Yin, C. Zhao, Y. Zhong, J. Liu, "Research on robust performance of speed-sensorless vector control for the induction motor using an interfacing multiple-model extended kalman filter", IEEE Transactions on Power Electronics, Vol. 29, No. 6, pp. 3011-3019, 2014

[3] K. Wang, W. Yao, K. Lee, Z. Lu, "Regenerating mode stability improvements for combined voltage and current mode flux observer in speed sensorless induction machine control", IEEE Transactions on Industry Applications, Vol. 50, No. 4, pp. 2564-2573, 2014

[4] G. Lefebvre, J. Gauthier, A. Hijazi, X. Lin-Shi, V. Digarcher, "Observability-index-based control strategy for induction machine sensorless drive at low speed", IEEE Transactions on Industrial Electronics, Vol. 64, No. 3, pp. 1929-1938, 2017

[5] R. Kumar, S. Das, P. Syam, A. K. Chattopadhyay, "Review on model reference adaptive system for sensorless vector control of induction motor drives", IET Electric Power Applications, Vol. 9, No. 7, pp. 496–511, 2015

[6] M. Zaky, M. Metwaly, "Sensorless torque/speed control of induction motor drives at zero and low frequency with stator and rotor resistance estimation", IEEE Journal of Emerging and Selected Topics in Power Electronics, Vol. 4, No. 4, pp 1416-1429, 2016

[7] W. Sun, J. Gao, Y. Yu, G. Wang, D. Xu, "Robustness improvement of speed estimation in speed-sensorless induction motor drives", IEEE

Transactions on Industry Applications, Vol. 52, No.3, pp. 2525-2536, 2016

[8] W. Pereira, C. Oliveira, M. Santana, T. de Almeida, A. de Castro, G. Paula, M. Aguiar, "Improved sensorless vector control of induction motor using sliding mode observer", IEEE Latin America Transactions, Vol. 14, No. 7, pp. 3110-3116, 2016

[9] A. Yepes, F. Baneira, J. Malvar, A. Vidal, D. Perez-Estévez, O. Lopez, J. Doval-Gandoy, "Selection criteria of multiphase induction machines for speed-sensorless drives based on rotor slot harmonics", IEEE Transactions on Industrial Electronics, Vol. 63, No. 8, pp. 4663-4673, 2016

[10] J. Arellano-Padilla, M. Sumner, C. Gerada, "Condition monitoring approach for permanent magnet synchronous motor drives based on the INFORM method", IET Electric Power Applications, Vol. 10, No. 1, pp. 54-62, 2016

[11] T. Lin, Z. Zhu, "Sensorless operation capability of surface-mounted permanent-magnet machine based on high-frequency signal injection methods", IEEE Transactions on Industry Applications, Vol. 51, No. 3, pp. 2161-2171, 2015

[12] X. Wang, W. Xie, G. Dajaku, R. M. Kennel, D. Gerling, R. D. Lorenz, "Position Self-Sensing Evaluation of Novel CW-IPMSMs With an HF Injection Method", IEEE Transactions on Industry Applications, Vol. 50, No. 5, pp. 3325-3334, 2014

[13] Q. Gao, G. Asher, M. Sumner, "Implementation of sensorless control of induction machines using only fundamental PWM waveforms of a two-level converter", IET Power Electronics, Vol. 6, No. 8, pp. 1575-1582, 2013

[14] E. Al-nabi, B. Wu, N. R. Zargari, V. Sood, "sensorless control of csc-fed ipm machine for zero- and low-speed operations using pulsating hfi method", IEEE Transactions on Industrial Electronics, Vol. 60, No. 5, pp. 1711-1723, 2013

[15] P. Landsmann, R. Kennel, "Saliency-based sensorless predictive torque control with reduced torque ripple", IEEE Transactions on Power Electronics, Vol. 27, No. 10, pp. 4311-4320, 2012

[16] M. Seilmeier, B. Piepenbreier, "Sensorless control of PMSM for the whole speed range using two-degree-of-freedom current control and hf test current injection for low-speed range", IEEE Transactions on Power Electronics, Vol. 30, No. 8, pp. 4394-4403, 2015

[17] Y. Yoon, S. Sul, "Sensorless Control for Induction Machines Based on Square-Wave Voltage Injection", IEEE Transactions on Power Electronics, Vol. 29, No. 7, pp. 3637-3645, 2014

[18] S. Yang, "Saliency-based position estimation of permanent-magnet synchronous machines using square-wave voltage injection with a single current sensor", IEEE Transactions on Industry Applications, Vol. 51, No. 2, pp. 1561-1571, 2015

[19] P. Xu, Z. Zhu, "Novel Square-Wave Signal Injection Method Using Zero-Sequence Voltage for Sensorless Control of PMSM Drives", IEEE Transactions on Industrial Electronics, Vol. 63, No. 12, pp. 7444-7454, 2016

[20] G. Xie, K. Lu, S. Dwivedi, R. Riber, W. Wu, "Permanent magnet flux online estimation based on zero-voltage vector injection method", IEEE Transactions on Power Electronics, Vol. 30, No. 12, pp. 6506-6509, 2015

[21] L. Harnefors, M. Hinkkanen, "Complete stability of reduced-order and full-order observers for sensorless IM drives", IEEE Transactions on Industrial Electronics, Vol. 55, No. 3, pp. 1319–1329, 2008

[22] M. Hinkkanen, "Stabilization of regenerating-mode operation in sensorless induction motor drives by full-order flux observer design", IEEE Transactions on Industrial Electronics, Vol. 51, No. 6, pp. 1318–1328, 2004

[23] M. Hinkkanen, "Analysis and design of full-order flux observers for sensorless induction motors", IEEE Transactions on Industrial Electronics, Vol. 51, No. 5, pp. 1033- 1040, 2004